Article

On the Effects of Geometry Control on the Performance of Overtopping Wave Energy Converters

Lander Victor [1,*], **Peter Troch** [1] **and Jens Peter Kofoed** [2]

[1] Department of Civil Engineering, Ghent University, Technologiepark 904, Zwijnaarde B-9052, Belgium; E-Mail: peter.troch@ugent.be

[2] Department of Civil Engineering, Aalborg University, Sohngaardsholmsvej 57, Aalborg DK-9000, Denmark; E-Mail: jpk@civil.aau.dk

* Author to whom correspondence should be addressed; E-Mail: lander.victor@ugent.be; Tel.: +32-9-264-5489; Fax: +32-9-264-5837.

Abstract: Overtopping wave energy converters (OWECs) are designed to extract energy from ocean waves based on wave overtopping into a reservoir, which is emptied into the ocean through a set of low-head turbines, and typically feature a low crest freeboard and a smooth impermeable steep slope. In the process of optimizing the performance of OWECs, the question arises whether adapting the slope geometry to the variable wave characteristics at the deployment site (*i.e.*, geometry control) can increase the overall hydraulic efficiency and overall hydraulic power compared to a fixed slope geometry. The effect of five different geometry control scenarios on the overall hydraulic efficiency and overall hydraulic power of OWECs has been simulated for three possible deployment sites using empirical prediction formulae. The results show that the effect of an adaptive slope angle is relatively small. On the other hand, adapting the crest freeboard of the OWECs to the wave characteristics increases the overall hydraulic efficiency and power. Based on the simulations, gains in overall hydraulic power of at least 30% are achievable when applying an adaptive crest freeboard compared to a fixed crest freeboard.

Glossary:

a_1, a_2	coefficients for empirical formula in Equation (10), values in Table 1 [-]
F_1, F_2	factors of Equation (11)
FO	frequency of occurrence of a sea state at a particular deployment site [%]
g	acceleration due to gravity [m/s^2]
h_t	water depth at the toe of the structure [m]
H_{m0}	spectral wave height of the incident waves at the toe of the structure [m]
$\widehat{H}_{m0}$	sea state averaged spectral wave height [m]
L_s	length of the slope of the OWEC [m]
m_{-1}	first negative moment of the incident wave spectrum [m^{2}s]
m_0	zeroth moment of the incident wave spectrum [m^2]
N_{SS}	number of sea states at a particular deployment site [-]
$OWECs$	Overtopping Wave Energy Converters
$P_{hydr,overall}$	overall hydraulic power [kW/m], *i.e.*, sum of hydraulic power over all sea states
P_{hydr}	hydraulic power for a particular sea state [kW/m]
P_{wave}	wave power for a particular sea state [kW/m]
q	average overtopping rate [m^3/s/m]
R_c	crest freeboard, *i.e.*, the vertical distance between the crest of the structure and the still water level [m]
$s_{m-1,0}$	wave steepness defined by $s_{m-1,0} = 2\pi H_{m0} / g T_{m-1,0}^2$ [-]
$\widehat{s}_{m-1,0}$	sea state average wave steepness [-]
S_1 to S_5	scenario 1 to scenario 5
$T_{m-1,0}$	spectral incident wave period at the toe of the structure defined by $T_{m-1,0} = m_{-1} / m_0$ [s]
x_{hinge}	horizontal dimension of the slope of the OWEC at the seabed [m]
α	slope angle of the structure [rad]
$\alpha_\circ$	slope angle of the structure [°]
$\eta_{hydr,overall}$	overall hydraulic efficiency [-], *i.e.*, sum of hydraulic efficiency over all sea states
η_{hydr}	hydraulic efficiency for a particular sea state [-]
λ_{dr}	correction coefficient for the draft of the structure by Kofoed (2002) [-]
λ_α	correction coefficient for the slope angle of the structure by Kofoed (2002) [-]
λ_s	correction coefficient for small relative crest freeboards by Kofoed (2002) [-]
ρ	density of water [kg/m^3] (1000 kg/m^3 for fresh water and 1025 kg/m^3 for salt water)
σ	standard deviation
$\xi_{m-1,0}$	breaker parameter, defined by $\xi_{m-1,0} = \tan\alpha / \sqrt{s_{m-1,0}}$ [-]

Subscripts:

j	sea state
pred	predicted
opt	maximum overall hydraulic efficiency

1. Introduction

The design of the slope geometry of an overtopping wave energy converter (OWEC) with a single level reservoir for a particular deployment site, characterized by a number (N_{SS} [-]) of characteristic sea states, is based on the maximization of the overall hydraulic efficiency $\eta_{hydr,overall}$ [-] [1,2]. This efficiency is defined as the sum of the hydraulic efficiencies $\eta_{hydr,j}$ [-] for each sea state (subscript j) at the deployment site, multiplied by the frequencies of occurrence FO_j [-] of the sea states [Equation (1)]:

$$\eta_{hydr,overall} = \sum_{j=1}^{N_{SS}} \eta_{hydr,j} FO_j \tag{1}$$

The hydraulic efficiency for a particular sea state $\eta_{hydr,j}$ is defined as the proportion of the hydraulic power $P_{hydr,j}$ [kW/m] to the wave power $P_{wave,j}$ [kW/m] for that sea state:

$$\eta_{hydr,j} = \frac{P_{hydr,j}}{P_{wave,j}} \tag{2}$$

The hydraulic power $P_{hydr,j}$ is defined as:

$$P_{hydr,j} = \rho g q_j R_{c,j} \tag{3}$$

where ρ [kg/m^3] is the water density, g [m/s^2] is the acceleration of gravity, q_j [m^3/s/m] is the average overtopping rate for sea state j and $R_{c,j}$ [m] is the crest freeboard (*i.e.*, the vertical distance between the still water level and the crest of the OWEC). The deep water definition is used for the wave power $P_{wave,j}$:

$$P_{wave,j} = \frac{\rho g^2}{64\pi} H_{m0,j}^2 T_{m-1,0,j} \tag{4}$$

in which H_{m0} [m] is the spectral wave height of the incident waves at the toe of the OWEC and $T_{m-1,0}$ [s] is spectral incident wave period at the toe of the OWEC defined by $T_{m-1,0} = m_{-1}/m_0$ (m_{-1} [m^{2}s] is the first negative moment of the incident wave spectrum and m_0 [m^2] is the zeroth moment of that spectrum).

The overall hydraulic power $P_{hydr,overall}$ [kW/m] is defined as:

$$P_{hydr,overall} = \sum_{j=1}^{N_{SS}} P_{hydr,j} FO_j \tag{5}$$

Based on Equation (1), the maximization of $\eta_{hydr,overall}$ for an OWEC with a fixed geometry results in fixed values of the slope angle and crest freeboard that are determined by the sea states with the largest frequencies of occurrence FO_j at the deployment site. Typically, those sea states contain relatively small amounts of energy. Hence, the geometry is not adapted to the more energetic sea states and their energy is not effectively captured.

Geometry control implies that the geometry of the slope is adapted to the characteristics of each sea state, in order to obtain a maximum hydraulic efficiency for each sea state, in contrast to a maximum

overall hydraulic efficiency for a fixed geometry. Consequently, the hydraulic efficiency $\eta_{hydr,j}$ [Equation (2)] needs to be maximized for each sea state. Hence, by applying geometry control, the energy of the less frequent, more energetic sea states is also captured maximally, resulting in a larger value of the overall hydraulic efficiency compared to a fixed geometry. Note that the crest freeboard $R_{c,j}$ also has a subscript j in Equation (3), since it depends on the sea state when using geometry control.

Based on Equations (2) and (3), knowledge on the average overtopping rate of OWECs with a single level reservoir is required in order to study the effect of geometry control on the overall hydraulic efficiency and power of these OWECs.

An important study on the overtopping behaviour of OWECs with a single level reservoir has been carried out by Kofoed [1]. The following empirical prediction formula has been proposed based on experimental tests with scale models of fixed OWECs characterized by a single uniform slope and mainly featuring a limited draft (slope not extending to the seabed):

$$\frac{q}{\sqrt{g\,H_{m0}^3}} = \lambda_{dr}\,\lambda_{\alpha}\,\lambda_{s}\,0.20\exp\left[(-2.6)\frac{R_c}{H_{m0}}\right] \qquad (6)$$

The corresponding ranges of application for the slope angle α [-] and the relative crest freeboard, defined as R_c / H_{m0} [-], are: $0.58 < \cot\alpha < 2.8$ and $0.15 < R_c / H_{m0} < 2.0$.

Basically, Equation (6) is based on Equation (7), where a number of correction coefficients have been added to align the formula with the experimental test results of Kofoed [1], extending the ranges of application of Equation (7) to steeper slopes and to smaller relative crest freeboards:

$$\frac{q}{\sqrt{g\,H_{m0}^3}} = 0.20\exp\left[(-2.6)\frac{R_c}{H_{m0}}\right] \qquad (7)$$

Equation (7) is a commonly used prediction formula for the average overtopping rates of mildly sloping dikes subjected to non-breaking waves [3,4]. The corresponding ranges of application for the slope angle and relative crest freeboard are: $1.0 < \cot\alpha < 4.0$ and $0.5 < R_c / H_{m0} < 3.5$. The reliability of Equation (7) is expressed by considering the coefficient -2.6 as a normally distributed stochastic variable with mean -2.6 and standard deviation $\sigma = 0.35$.

The effect of the limited draft on the average overtopping rate is taken into account in Equation (6) by the coefficient λ_{dr} [-], which equals 1.0 when the slope extends to the seabed. The dimensionless coefficient λ_{α} [-], defined in Equation (8), expresses an observed decrease in average overtopping rate for slope angles $\alpha_{\circ}$ [°] deviating from $\cot\alpha = 1.7$ ($\alpha_{\circ} = 30°$), while the coefficient λ_s [-] compensates for an observed overestimation of the average overtopping rate by Equation (7) for relative crest freeboards $R_c / H_{m0} < 0.75$ [Equation (9)]. λ_s has been calibrated using test results of Schüttrumpf [5] for structures with a zero crest freeboard and with $3.0 \leq \cot\alpha \leq 6.0$:

$$\lambda_{\alpha} = \left[\cos\left(\alpha_{\circ} - 30°\right)\right]^3 \qquad (8)$$

$$\lambda_s = \begin{cases} 0.40\sin\left(\dfrac{2}{3}\pi\dfrac{R_c}{H_{m0}}\right)+0.60 & \dfrac{R_c}{H_{m0}}<0.75 \\[4mm] 1.0 & \dfrac{R_c}{H_{m0}}\geq 0.75 \end{cases} \tag{9}$$

Another study, applicable to single reservoir OWECs, has been recently carried out by Victor and Troch [6]. Average overtopping rates have been measured for smooth impermeable steep sloping structures with low crest freeboards and a slope extending to the seabed ($\lambda_{dr}=1.0$), subjected to non-breaking waves. The corresponding test set-up has been described in detail by Victor and Troch [7]. The test results have been gathered in a dataset (referred to as the UG10 dataset) with the following ranges of application for the slope angle α, relative crest freeboard R_c/H_{m0} and wave steepness $s_{m-1,0}$ [-] (defined as $2\pi H_{m0}/gT_{m-1,0}^2$): $0.36<\cot\alpha<2.8$, $0.11<R_c/H_{m0}<1.7$ and $0.015<s_{m-1,0}<0.050$. Note that the tested range of wave steepness is not valid for swells.

These broad ranges of application allowed to study the effects of these parameters on the average overtopping rates of steep low-crested structures (Victor and Troch [6]). The largest average overtopping rate $q/\sqrt{gH_{m0}^3}$ occurs for slopes with $\cot\alpha>1.5$, which exhibit only a small effect of the slope angle. For $\cot\alpha<1.5$, a significant decrease in average overtopping rate occurs towards the rate for vertical walls with non-impacting wave attack [4,8]. Furthermore, a decrease in the relative crest freeboard results in an increase in $q/\sqrt{gH_{m0}^3}$. This increase is larger for $R_c/H_{m0}>0.8$ than for $R_c/H_{m0}\leq 0.8$. The smaller effect of the relative crest freeboard for small relative crest freeboards is also suggested by λ_s. However, this parameter describes the reduced effect insufficiently, since it is based on test results with relatively mild slopes (1:3 to 1:6) for a zero crest freeboard. The effect of the relative crest freeboard on $q/\sqrt{gH_{m0}^3}$ increases for increasing slope angle.

The effect of the wave period appears to be small compared to the effects of the slope angle and relative crest freeboard.

Finally, a set of prediction formulae has been proposed, based on the new experimental test results (UG10 dataset), and based on test results available in literature for vertical walls subjected to non-impacting waves and for steep sloped structures with zero crest freeboard.

The test results of the UG10 dataset with $\cot\alpha>1.5$ have been studied in detail recently. Since these test results correspond to the largest average overtopping rates, accurate predictions of these rates are required in order to find the OWEC configuration with the maximum average overtopping rate. The detailed study resulted in a set of more accurate prediction formulae compared to the formulae suggested by Victor and Troch [6] for the average overtopping rates of steep low-crested structures with $1.5<\cot\alpha<2.8$:

$$\frac{q}{\sqrt{gH_{m0}^3}}=a_1\left[\cos\left(\frac{\xi_{m-1,0}-3.0}{3.0}\right)\right]^3 \exp\left(a_2\frac{R_c}{H_{m0}}\right) \tag{10}$$

with coefficients a_1 [-] and a_2 dependent on the value of the relative crest freeboard (Table 1). $\xi_{m-1,0}$ [-] is the breaker parameter, defined by $\xi_{m-1,0}=\tan\alpha/\sqrt{s_{m-1,0}}$. Non-breaking waves occur for $\xi_{m-1,0}>2.0$ [4].

Table 1. Values of the coefficients and reliability of Equation (10).

Relative Crest Freeboard	a_1	a_2	σ
$R_c / H_{m0} \leq 0.8$	0.10	-1.8	0.057
$R_c / H_{m0} > 0.8$	0.091	-1.7	0.12

The reliability of Equation (10) is expressed by considering the logarithm of the dimensionless average overtopping rate as a normally distributed stochastic variable with the logarithm of the predicted dimensionless average overtopping rate by Equation (10) as a mean and a standard deviation σ given in Table 1. The standard deviation depends on the value of the relative crest freeboard.

The following important remarks are made regarding geometry control:

- the optimal geometry is determined based on a maximization of the hydraulic efficiency. The total efficiency of an OWEC is also determined by the efficiency of the reservoir, turbines efficiency and generator efficiency. However, these efficiencies are not considered when designing the optimal slope geometry;

- geometry control requires the adaptation of the geometry to each sea state. This involves that part of the power which is gained from the ocean waves is not transferred to the grid but is used to carry out the adaptations of the slope geometry;

- when a location is dominated by one sea state, geometry control is not effective.

The main goal of this paper is to verify whether applying geometry control results in an increase in the overall hydraulic efficiency and overall hydraulic power for OWECs with a single level reservoir and a slope extending to the seabed. The formulae given above [Equation (10)] enable to determine the optimal geometry for each sea state, resulting in the maximum hydraulic efficiency [Equation (2)] for that sea state (only wind seas, no swells). This aspect is discussed in the first section below (Section 2). The effect of five different geometry control scenarios on the overall hydraulic efficiency of OWECs has been studied at three possible deployment sites (Section 4). The scenarios are described in Section 3, while the data for the deployment sites are given in Section 4. The effect of geometry control on the overall hydraulic power of OWECs has been studied as well, since power is more tangible than efficiency.

2. Optimal Geometry for a Sea State

2.1. General

The optimal geometry for a sea state consists of the values of $\cot\alpha_j$ and $R_{c,j}$ which lead to a maximum hydraulic efficiency [Equation (2)]. A maximization of the right hand side of Equation (2) requires a maximization of the product $q_j R_{c,j}$, with q_j being dependent on $\cot\alpha_j$ and $R_{c,j}$ as illustrated in Equation (10). Note that this also results in a maximization of the hydraulic power, *i.e.*, the numerator of the right hand side of Equation (2).

It is clear that the crest freeboard plays an important role in maximizing $q_j R_{c,j}$. When using a low crest freeboard, large average overtopping rates occur, but with rather low potential energy, resulting in low values of the hydraulic efficiency. On the other hand, a high crest freeboard increases the

potential energy of the overtopping water, but the amount of overtopping is reduced. Consequently, an optimum crest freeboard exists, for which the average overtopping rate q_j needs to be maximized. Since the largest average overtopping rates occur for $1.5 < \cot\alpha < 2.8$, independent of the value of the relative crest freeboard [6], the set of prediction formulae in Equation (10) should be applied. Based on Equation (10), the following expression is valid for $q_j R_{c,j}$:

$$q_j R_{c,j} = F_1 F_2 \tag{11a}$$

where:

$$F_1 = \left[\cos\left(\frac{\xi_{m-1,0,j} - 3.0}{3.0} \right) \right]^3 \tag{11b}$$

$$F_2 = a_1 \exp\left(a_2 \frac{R_{c,j}}{H_{m0,j}} \right) R_{c,j} \sqrt{g H_{m0}^3} \tag{11c}$$

Since the effect of the slope angle and crest freeboard are independent in Equation (11), the optimal values of both parameters are determined independent from each other. The optimal slope angle is based on a maximization of the factor $F_1 = \left[\cos\left(\left(\xi_{m-1,0,j} - 3.0 \right)/3.0 \right) \right]^3$. This introduces the concept of an adaptive slope angle (Section 2.2).

The optimal crest freeboard maximizes the factor $F_2 = a_1 \exp\left(a_2 R_{c,j}/H_{m0,j} \right) R_{c,j} \sqrt{g H_{m0}^3}$, which introduces the concept of an adaptive crest freeboard (Section 2.3).

2.2. Adaptive Slope Angle

It is clear that the factor F_1 is maximal when the breaker parameter $\xi_{m-1,0,j}$ takes the value 3.0. This requirement for the breaker parameter determines the optimal slope angle for a specific sea state [Equation (12)], resulting in the maximum average overtopping rate for that particular sea state and a specific crest freeboard:

$$\tan\alpha_{j,opt} = 3.0\sqrt{s_{m-1,0,j}} \tag{12}$$

Note that the optimal slope angle only depends on the wave steepness of the sea state. When the waves are steeper, the optimal slope is also steeper. The concept of an adaptive slope angle consists of applying the optimal slope angle determined using Equation (12) for each of the characteristic sea states of a deployment site.

Deployment of the steep low-crested slopes with a fixed crest freeboard in a location at sea with little variation in wave steepness consequently results only in a small gain in performance when applying an adaptive slope angle compared to a fixed slope angle.

2.3. Adaptive Crest Freeboard

The optimal crest freeboard is determined by maximizing the factor F_2. This is achieved by setting the derivative of F_2 to $R_{c,j}$ equal to zero:

$$\frac{dF_2}{dR_{c,j}} = 0 \tag{13}$$

$$\Rightarrow \frac{d\left(\sqrt{g H_{m0,j}^3}\, a_1\, R_{c,j}\, \exp\left(a_2\, \dfrac{R_{c,j}}{H_{m0,j}} \right) \right)}{dR_{c,j}} = 0 \tag{14}$$

$$\Rightarrow \exp\left(a_2\, \frac{R_{c,j}}{H_{m0,j}} \right)\left[a_1 + a_1\, R_{c,j}\, \frac{a_2}{H_{m0,j}} \right] = 0 \tag{15}$$

$$\Rightarrow \left[a_1 + a_1\, R_{c,j}\, \frac{a_2}{H_{m0,j}} \right] = 0 \tag{16}$$

$$\Rightarrow \left(\frac{R_{c,j}}{H_{m0,j}} \right)_{opt} = \frac{-1}{a_2} \tag{17}$$

The coefficient a_2 takes the value -1.8 for $R_c / H_{m0} \leq 0.8$, while it is -1.7 for $R_c / H_{m0} > 0.8$. Since the optimal relative crest freeboard [Equation (17)] is smaller than 0.8 for both values of a_2, the value of the optimal crest freeboard becomes:

$$\left(\frac{R_{c,j}}{H_{m0,j}} \right)_{opt} = 0.56 \tag{18}$$

The analytically obtained value of the optimal relative crest freeboard [Equation (18)] is confirmed by plotting the hydraulic efficiency [Equation (2)] as a function of the relative crest freeboard for test results of the UG10 dataset, for example with slope angle $\cot\alpha = 1.4$ and a breaker parameter $\xi_{m-1,0} \approx 3.0$ (Figure 1). The maximum hydraulic efficiency for the example in Figure 1 occurs for a relative crest freeboard $R_c / H_{m0} \approx 0.56$.

An adaptive relative crest freeboard implies that the crest freeboard of steep low-crested slopes is adapted for each sea state, based on the condition that $\left(R_{c,j} / H_{m0,j} \right)_{opt} = 0.56$.

The prediction formulae in Equations (6) and (7) could also be used to predict the average overtopping rate, resulting in different values of the optimal relative crest freeboard. When applying Equation (7), an optimal relative crest freeboard of $1/2.6 = 0.38$ is found. The larger value of $\left(R_{c,j} / H_{m0,j} \right)_{opt}$ in Equation (18) is caused by the deviation of the test results of the UG10 dataset below the prediction line of Equation (7) for relative crest freeboards R_c / H_{m0} smaller than 0.8 (e.g., Figure 2).

Figure 1. Graph of hydraulic efficiency as a function of the relative crest freeboard, for test results of the UG10 dataset with $\cot\alpha = 1.4$ and $\xi_{m-1,0} = 3.0$.
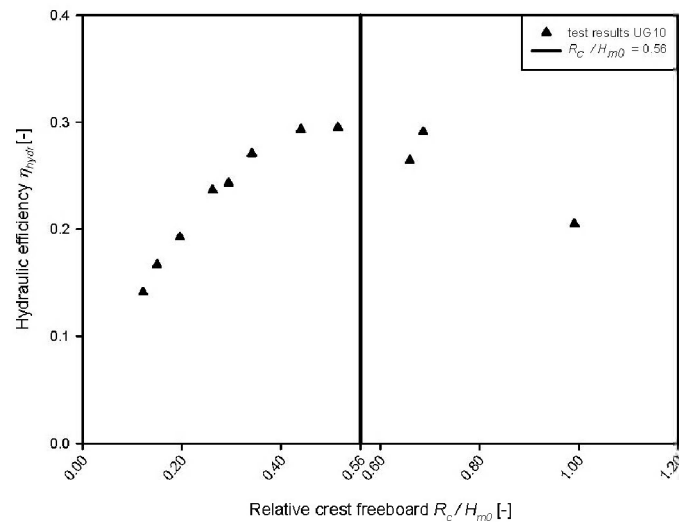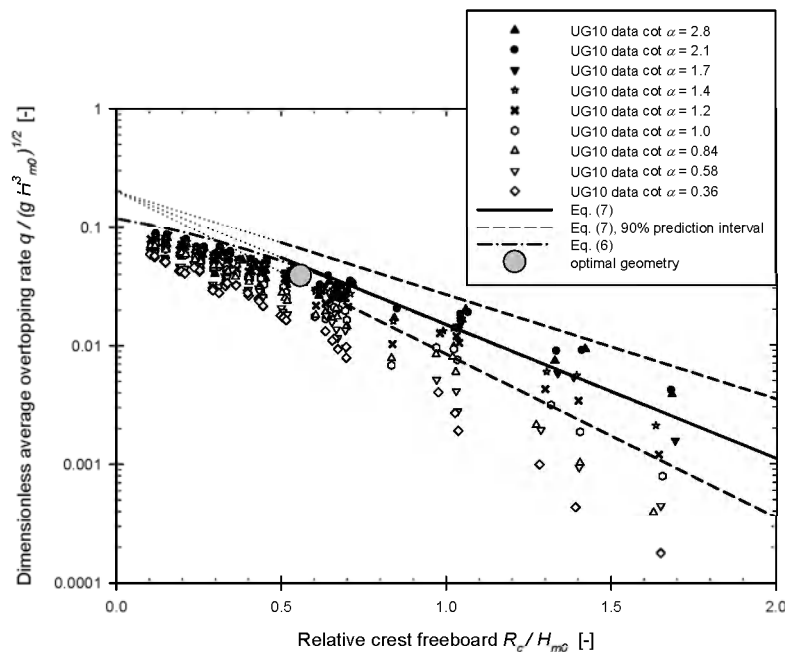

Figure 2. Log-linear graph of dimensionless average overtopping rate (logarithmic scale) as a function of the relative crest freeboard (linear scale) for the test results of the UG10 dataset, with R_c / H_{m0} varying between 0.0 and 2.0. Grey dot indicates the point of optimal geometry.

The optimal relative crest freeboard predicted based on Equation (6) [1], assuming the correction factors λ_{dr} and λ_α are equal to 1.0, is expected to be closer to 0.56, since this formula takes into account a deviation below Equation (7) for smaller relative crest freeboards, through the use of λ_s [(Equation (9)]. The optimal relative crest freeboard based on Equation (6) is derived as follows:

$$\frac{d\left(\sqrt{gH_{m0,j}^3}\,\lambda_{s,j}\,0.20\exp\left((-2.6)\dfrac{R_{c,j}}{H_{m0,j}}\right)R_{c,j}\right)}{dR_{c,j}} = 0 \tag{19a}$$

$$\Rightarrow \left(R_{c,j}\,/\,H_{m0,j}\right)_{opt} = 0.48 \tag{19b}$$

The value of the optimal relative crest freeboard in Equation (19b) is indeed larger than 0.38 and tends towards the value of 0.56 in Equation (18).

2.4. Hydraulic Efficiency for Optimal Geometry

Based on Sections 2.2 and 2.3, the optimal geometry which results in maximum hydraulic efficiency for a particular sea state is achieved when: $\tan\alpha_j = 3.0\sqrt{s_{m-1,0,j}}$ and $R_{c,j}\,/\,H_{m0,j} = 0.56$. Since $\left(R_{c,j}\,/\,H_{m0,j}\right)_{opt} < 0.8$, the optimal geometry corresponds to a dimensionless average overtopping rate expressed by:

$$\left(q_j\,/\,\sqrt{gH_{m0,j}^3}\right)_{opt} = 0.1\exp\left(-1.8\cdot0.56\right) = 0.38 \tag{20}$$

This value of $q/\sqrt{gH_{m0}^3}$ is referred to as the *optimal dimensionless average overtopping rate*. The corresponding point of optimal geometry is indicated with a grey dot in Figure 2, which shows all dimensionless average overtopping rates of the UG10 dataset as a function of the relative crest freeboard, together with the predictions by Equations (6) and (7). Successively, the expression for the maximum hydraulic efficiency at the point of optimal geometry is derived as:

$$\left(\eta_{hydr,j}\right)_{opt} = \frac{\rho g\left[\sqrt{gH_{m0,j}^3}\,0.038\right]R_{c,j}}{\dfrac{\rho g^2}{64\pi}H_{m0,j}^2\,T_{m-1,0,j}} \tag{21a}$$

$$= \frac{\left[\sqrt{H_{m0,j}}\,0.038\right]0.56}{\dfrac{\sqrt{g}}{64\pi}T_{m-1,0,j}} \tag{21b}$$

$$= 1.7\sqrt{s_{m-1,0,j}} \tag{21c}$$

It appears that the maximum hydraulic efficiency for a specific sea state only depends on the wave steepness of that sea state. When the waves are steeper, the maximum hydraulic efficiency will be larger.

3. Geometry Control—Different Scenarios

Applying the optimal geometry derived in Section 2 to the different characteristic sea states at a particular deployment site (*i.e.*, geometry control in its strict sense), requires an adaptation of both the slope angle and crest freeboard to its optimal values for each sea state. The OWECs studied in this

paper however are less flexible concerning geometry control compared to floating OWECs. Hence, realizing such adaptation in practice is not straightforward.

Therefore, a number of additional geometry control scenarios are suggested. These scenarios violate the strict definition of geometry control, thus resulting in a hydraulic efficiency which is smaller than the maximum hydraulic efficiency derived in Section 2.4. In total, five geometry control scenarios have been used in this paper to investigate the effect of geometry control on the overall hydraulic efficiency and the overall hydraulic power. Each of these scenarios is described below.

3.1. Scenario 1: Adaptive Slope Angle and Adaptive Crest Freeboard (S1)

An optimal geometry is applied for each sea state: $\tan \alpha_j = 3.0 \sqrt{s_{m-1,0,j}}$ and $R_{c,j} / H_{m0,j} = 0.56$ for each j. This scenario requires a vertical motion of the crest of the structure and a rotation of the slope independent of the crest freeboard (Figure 3). The combination of these movements is not straightforward in practice.

Figure 3. Scenario 1—Geometry control by adaptive slope angle and adaptive crest freeboard (S1).
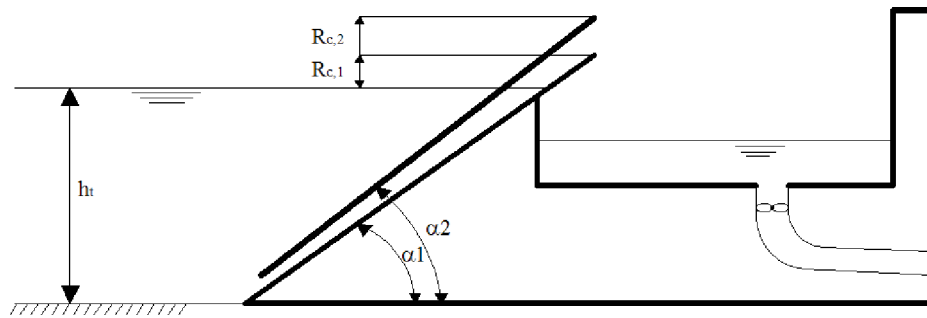

3.2. Scenario 2: Adaptive Slope Angle (S2)

In this scenario, an adaptive slope angle is applied only, fulfilling the condition $\tan \alpha_j = 3.0 \sqrt{s_{m-1,0,j}}$, in combination with a fixed crest freeboard (Figure 4). The variation in slope angle is achieved by applying a hinge point at the crest of the slope. The value of the fixed crest freeboard is based on a maximization of the overall hydraulic efficiency, as expressed in Equations (22) and (23):

$$\frac{d\eta_{hydr,overall}}{dR_c} = 0 \tag{22}$$

$$\Rightarrow \frac{d}{dR_c} \left(\sum_{j=1}^{N_{ss}} \frac{\rho g \, q_j \, R_c \, FO_j}{P_{wave,j}} \right) = 0 \tag{23}$$

Figure 4. Scenario 2—Geometry control by adaptive slope angle (S2).
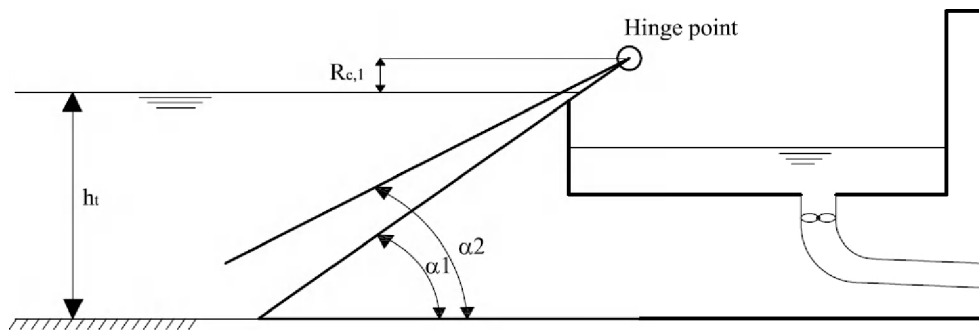
The fixed crest freeboard is not optimal for each sea state, and it is unclear whether it is smaller or larger than $R_{c,j} / H_{m0,j} = 0.8$. Taking into account the fulfilment of the condition $\tan \alpha_j = 3.0 \sqrt{s_{m-1,0,j}}$ for scenario 2, the average overtopping rate thus is expressed by:

$$q_j = a_{1,j} \exp \left(a_{2,j} \frac{R_c}{H_{m0,j}} \right) \sqrt{g H_{m0,j}^3} \tag{24}$$

Hence, Equation (23) can be rewritten as:

$$\frac{d}{dR_c} \left(\sum_{j=1}^{N_{SS}} \frac{\left[a_{1,j} \exp \left(a_{2,j} \frac{R_c}{H_{m0,j}} \right) \right] \sqrt{g H_{m0,j}^3} R_c FO_j}{P_{wave,j}} \right) = 0 \tag{25}$$

$$\Rightarrow \sum_{j=1}^{N_{SS}} \frac{q_j FO_j}{P_{wave,j}} \left[a_{2,j} \frac{R_c}{H_{m0,j}} + 1 \right] = 0 \tag{26}$$

The coefficients $a_{1,j}$ and $a_{2,j}$ depend on the relative crest freeboard (Table 1). The fixed crest freeboard for scenario 2 is found by solving Equation (26) for R_c, using numerical methods that are implemented in MS Excel© (Solver add-in) and in Maple™ (fsolve function). The resulting fixed crest freeboard is largely determined by the sea states with the largest frequencies of occurrence and approaches the optimal crest freeboards for those sea states relatively closely.

3.3. Scenario 3: Adaptive Crest Freeboard (S3)

This scenario combines a fixed slope angle with the optimal crest freeboard for each sea state, *i.e.*, fulfilling the condition $R_{c,j} / H_{m0,j} = 0.56$ (Figure 5). The value of the fixed slope angle is determined by maximizing the overall hydraulic efficiency [Equations (27) and (28)]:

$$\frac{d\eta_{hydr,overall}}{d \tan \alpha} = 0 \tag{27}$$

$$\Rightarrow \frac{d}{d \tan \alpha} \left(\sum_{j=1}^{N_{SS}} \frac{\rho g q_j R_{c,j} FO_j}{P_{wave,j}} \right) = 0 \tag{28}$$

Figure 5. Scenario 3—Geometry control by adaptive crest freeboard (S3).
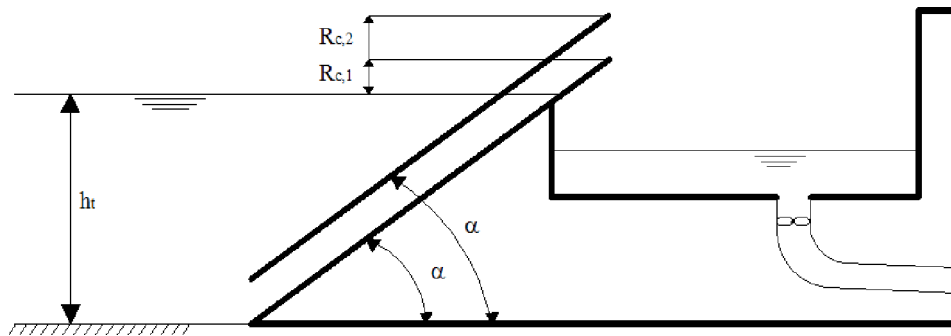
The fixed slope angle is not optimal for each sea state. However, since the optimal slopes for each of the different sea states range between $\cot\alpha = 1.5$ and $\cot\alpha = 3.0$ roughly, the differences between the optimal slope angles and the fixed slope angle for scenario 3 are relatively small. Hence, Equation (28) can be rewritten as:

$$\Rightarrow \sum_{j=1}^{N_{SS}} \frac{\left[0.1\exp\left(-1.8\frac{R_{c,j}}{H_{m0,j}}\right)\right] R_{c,j}\, FO_j \sqrt{g\,H_{m0}^3}}{P_{wave,j}} \frac{d}{d\tan\alpha}\left(\cos\left(\frac{\frac{\tan\alpha}{\sqrt{s_{m-1,0,j}}}-3.0}{3.0}\right)\right)^3 = 0 \qquad (29)$$

$$\Rightarrow \sum_{j=1}^{N_{SS}} \frac{q_j\, FO_j}{P_{wave,j}}\left[\frac{R_{c,j}}{\sqrt{s_{m-1,0,j}}}\left(-\tan\left(\frac{\frac{\tan\alpha}{\sqrt{s_{m-1,0,j}}}-3.0}{3.0}\right)\right)\right] = 0 \qquad (30)$$

The fixed slope angle for scenario 3 is found by solving Equation (30) for $\tan\alpha$, using numerical methods (MS Excel© and Maple™). Intrinsically, the fixed slope angle is determined by the sea states with the largest frequencies of occurrence. Although this geometry control strategy is simpler compared to scenario 1, realizing the vertical movement of the crest of the slope required for scenario 3 is also not straightforward in practice.

3.4. Scenario 4: Fixed Slope Angle and Fixed Crest Freeboard (S4)

In this particular scenario, no geometry control is applied (Figure 6). The values of the fixed slope angle and crest freeboard are determined by maximizing the overall hydraulic efficiency. This means that the partial derivatives of the overall hydraulic efficiency for the slope angle and the crest freeboard should be zero [Equation (31)]:

$$\left.\begin{array}{l} \dfrac{\partial}{\partial\tan\alpha}\left(\displaystyle\sum_{j=1}^{N_{SS}}\dfrac{\rho g\, q_j\, R_c\, FO_j}{P_{wave,j}}\right)=0 \\[4mm] \dfrac{\partial}{\partial R_c}\left(\displaystyle\sum_{j=1}^{N_{SS}}\dfrac{\rho g\, q_j\, R_c\, FO_j}{P_{wave,j}}\right)=0 \end{array}\right\} \qquad (31)$$

Figure 6. Scenario 4—No geometry control—Fixed slope angle and fixed crest freeboard (S4).

Based on Equations (26) and (30), this system can be rewritten as:

$$\begin{cases} \sum_{j=1}^{N_{SS}} \frac{q_j \, FO_j}{P_{wave,j}} \left[\frac{R_c}{\sqrt{s_{m-1,0,j}}} \left(-\tan\left(\frac{\frac{\tan\alpha}{\sqrt{s_{m-1,0,j}}} - 3.0}{3.0} \right) \right) \right] = 0 \\[2em] \sum_{j=1}^{N_{SS}} \frac{q_j \, FO_j}{P_{wave,j}} \left[a_{2,j} \frac{R_c}{H_{m0,j}} + 1 \right] = 0 \end{cases} \tag{32}$$

The fixed slope angle and crest freeboard for scenario 4 are found by solving the system in Equation (32) for $\tan\alpha$ and R_c. The system can be solved by using numerical methods, based on a minimization of the sum of squares of the left hand sides of the two equations in the system.

3.5. Scenario 5: Adaptive Crest Freeboard, Hinge at Bottom (S5)

In this scenario, the adaptive crest freeboard is realized by using a hinge point at the bottom of the slope (Figure 7), which results in a combined control of the slope angle and the crest freeboard.

Figure 7. Scenario 5—Geometry control by installing a hinge point at the bottom of the slope—determining parameters (S5).

An increase in wave height results in an increase in the optimal crest freeboard [Equation (18)] ($R_{c,1}$ to $R_{c,2}$) and, in correspondence to Figure 7, the slope becomes steeper (α_1 to α_2). Since an increase in wave height also corresponds to an increase in the optimal slope angle [Equation (12)],

the installation of the hinge at the bottom of the slope has a positive effect on the overall hydraulic efficiency.

The slope angles are directly related to the length of the slope, denoted by L_S, through Equation (33) or Equation (34), based on trigonometry:

$$\sin\alpha_j = \frac{h_t + R_{c,j}}{L_s} \tag{33}$$

$$\tan\alpha_j = \frac{h_t + R_{c,j}}{\sqrt{L_s^2 - \left(h_t + R_{c,j}\right)^2}} \tag{34}$$

The fixed slope length is determined by a maximization of the overall hydraulic efficiency. Accordingly, the constant value of L_s is found by setting the derivative equal to zero [Equations (35) and (36)], similar to Sections 3.2 and 3.3:

$$\frac{d\eta_{hydr,overall}}{dL_s} = 0 \tag{35}$$

$$\Rightarrow \frac{d}{dL_s}\left(\sum_{j=1}^{N_{ss}} \frac{\rho g\, q_j\, R_{c,j}\, FO_j}{P_{wave,j}}\right) = 0 \tag{36}$$

Applying the expression for the average overtopping rate for $R_c / H_{m0} \leq 0.8$ and taking into account Equation (34), Equation (36) can be rewritten as:

$$\sum_{j=1}^{N_{ss}} \frac{\left[0.1\exp\left(-1.8\dfrac{R_{c,j}}{H_{m0,j}}\right)\right] R_{c,j}\, FO_j \sqrt{g\,H_{m0,j}^3}}{P_{wave,j}} \frac{d}{dL_s}\left(\cos\left(\frac{\dfrac{h_t + R_{c,j}}{\sqrt{L_s^2 - \left(h_t + R_{c,j}\right)^2}\sqrt{s_{m-1,0,j}}} - 3.0}{3.0}\right)\right)^3 = 0 \tag{37}$$

$$\Rightarrow \sum_{j=1}^{N_{ss}} \frac{q_j\, FO_j}{P_{wave,j}}\left[\frac{R_{c,j}\left(h_t + R_{c,j}\right)L_s}{\left(L_s^2 - \left(h_t + R_{c,j}\right)^2\right)^{3/2}\sqrt{s_{m-1,0,j}}}\tan\left(\frac{\dfrac{h_t + R_{c,j}}{\sqrt{L_s^2 - \left(h_t + R_{c,j}\right)^2}\sqrt{s_{m-1,0,j}}} - 3.0}{3.0}\right)\right] = 0 \tag{38}$$

The fixed slope length for scenario 5 is found by solving Equation (38) for L_S, using numerical methods. Once the fixed slope length is known, the position of the hinge point is determined by the smallest crest freeboard $R_{c,1}$, corresponding to sea state 1:

$$x_{hinge} = \sqrt{L_s^2 - \left(h_t + R_{c,1}\right)^2} \tag{39}$$

The origin of the horizontal distance x_{hinge} is positioned at the intersection of the vertical line through the crest of the slope corresponding to sea state 1 and the sea bottom (Figure 7).

3.6. Overview of Scenarios

Table 2 summarizes the characteristics of the five scenarios described above.

Table 2. Characteristics of the five scenarios of geometry control.

Scenario No.	Acronym	Slope Angle	Crest Freeboard
1	S1	Adaptive	Adaptive
2	S2	Adaptive	Fixed
3	S3	Fixed	Adaptive
4	S4	Fixed	Fixed

4. Application to a Number of Possible Deployment Sites

Each of the five scenarios described in Section 3 has been applied to a number of possible deployment sites (Section 4.1), in order to study the effect of geometry control on the overall hydraulic efficiency (Section 4.3) and the overall hydraulic power (Section 4.4). Since scenario 4 corresponds to a fixed geometry, the outcomes of the four other scenarios are compared to that scenario.

The simulations for the three possible deployments sites are carried out using the formulae which are based on the UG10 dataset. It is again emphasized that those formulae are only applicable to sheltered areas, since the values of the wave steepness used during the UG10 test series are only valid for wind seas [7]. Hence, the formulae are not applicable to OWECs positioned in swells.

4.1. Chosen Deployment Sites

Three nearshore locations have been chosen (Table 3): Ostend (Belgian Continental Shelf), MPN (Dutch Continental Shelf) and Fjaltring (Danish Continental Shelf). All three locations are located relatively close to shore, in areas which are not exposed to large swells due to the sheltering effect of the UK from large period ocean waves.

Table 3. Important characteristics for three possible deployment sites.

Deployment Site	Average Annual Available Wave Power [kW/m]	Mean Water Depth [m]	Shortest Distance to Shore [km]	Data Acquisition Period
Ostend, BE	1.7	6.0	1	1997–2005
MPN, NL	5.4	18	8	1979–2002
Fjaltring, DK	7.0	20	4	1979–1993

Research on the wave characteristics for these three locations has been carried out based on the analysis of signals of wave measurement equipment, gathered during a relatively long time. The acquisition periods for the wave data used below for the three possible deployment sites are added to Table 3. The average annual available wave power in Ostend is rather low, while the wave power at MPN and Fjaltring is larger. Omnidirectional annual average scatter diagrams are available for the three possible deployment sites, allowing to determine the characteristic sea states for each of the three locations. These sea states are given below in Table 4 (Ostend), Table 5 (MPN) and Table 6 (Fjaltring).

Table 4. Characteristic sea states for location on the Belgian Continental Shelf (Ostend), $h_t = 6$ m, source scatter diagram: Flemish Ministry of Transport and Public Works, Agency for Maritime and Coastal Services—Coastal Division.

ID Sea State j	1	2	3	4	5
$H_{m0,j}$ [m]	0.25	0.75	1.25	1.75	2.25
$T_{m-1,0}$ [s]	4.19	4.60	5.18	5.94	6.59
$P_{wave,j}$ [kW/m]	0.1	1.2	3.9	8.7	16.0
FO_j [%]	49.20	35.89	10.12	3.08	1.18
$s_{m-1,0,j}$ [-]	0.009	0.023	0.030	0.032	0.033

Table 5. Characteristic sea states for location on the Dutch Continental Shelf (MPN), $h_t = 18$ m, source scatter diagram: Rijkswaterstaat [9].

ID Sea State j	1	2	3	4
$H_{m0,j}$ [m]	0.5	1.5	2.5	3.5
$T_{m-1,0}$ [s]	4.62	5.49	6.49	7.46
$P_{wave,j}$ [kW/m]	0.55	5.91	19.41	43.76
FO_j [%]	59.84	30.42	7.70	1.64
$s_{m-1,0,j}$ [-]	0.015	0.032	0.038	0.040

Table 6. Characteristic sea states for location on Danish Continental Shelf (Fjaltring), $h_t = 20$ m, source scatter diagram: Ramboll *et al.* [10].

ID Sea State j	1	2	3	4	5	6	7	8
$H_{m0,j}$ [m]	0.25	0.75	1.25	1.75	2.25	2.75	3.25	3.75
$T_{m-1,0}$ [s]	3.76	4.56	5.19	5.94	6.56	7.34	7.78	8.41
$P_{wave,j}$ [kW/m]	0.1	1.3	4.0	8.9	16.3	27.2	40.3	58.0
FO_j [%]	20.8	31.5	20.1	11.9	7.1	4.4	2.5	1.2
$s_{m-1,0,j}$ [-]	0.011	0.023	0.030	0.032	0.033	0.033	0.034	0.034

The energy period $T_{m-1,0}$ is taken for the wave period characterizing the sea states, since the energy period is present in the prediction formulae described in Section 1. Note that for all these three locations, the sea states with the smallest wave power are most dominantly present. The sea states with the largest power only occur during a limited amount of time.

4.2. Fixed Geometry Components for Scenarios 2 to 5

In order to derive the overall hydraulic efficiency $\eta_{hydr,overall}$ and the overall hydraulic power $P_{hydr,overall}$ for scenarios 2 to 5, the fixed geometry components for these scenarios have been determined based on the formulae in Section 3 (Table 7).

Table 7. Fixed geometrical parameters for scenarios 2 to 5 at the three possible deployment sites.

Deployment Site	Fixed Crest Freeboard Scenario 2 [m]	Cotangent Fixed Slope Angle Scenario 3 [-]	Fixed Crest Freeboard Scenario 4 [m]	Cotangent Fixed Slope Angle Scenario 4 [-]	Fixed Slope Length Scenario 5 [m]
Ostend, BE	0.25	2.80	0.25	2.80	21.48
MPN, NL	0.40	2.37	0.39	2.43	47.41
Fjaltring, DK	0.53	2.21	0.57	2.06	43.80

The values of the geometrical parameters in Table 7 are largely determined by the approximate fulfilment of the optimal conditions $\tan \alpha_j = 3.0 \sqrt{s_{m-1,0,j}}$ and $R_{c,j} / H_{m0,j} = 0.56$ for the sea states with the largest frequencies of occurrence. The differences between the three locations are thus explained based on parameters that represent the wave characteristics of the most frequents sea states for a particular location. Therefore, a sea state averaged wave height [Equation (40)] and sea state averaged wave steepness [Equation (41)] have been defined. The corresponding values for the three possible deployment sites are given in Table 8:

$$\widehat{H}_{m0} = \sum_{j}^{n} H_{m0,j} FO_j \qquad (40)$$

$$\widehat{s}_{m-1,0} = \sum_{j}^{n} s_{m-1,0,j} FO_j \qquad (41)$$

Table 8. Sea state averaged wave height and wave steepness for different test locations.

Deployment Site	$\widehat{H}_{m0}$	$\widehat{s}_{m-1,0}$
Ostend, BE	0.60	0.0002
MPN, NL	1.01	0.0222
Fjaltring, DK	1.15	0.0245

In accordance with Equation (12), a larger sea state averaged wave steepness should correspond to a larger value of the fixed slope angle. Furthermore, an increase in the sea state averaged wave height is expected to cause an increase in the fixed relative crest freeboard, based on Equation (18). This is confirmed when comparing Tables 7 and 8. The fixed crest freeboard increases when moving from Ostend to MPN and to Fjaltring, both for scenarios 2 and 4, corresponding to the increase in sea state averaged wave height shown in Table 8. The optimal slope angle increases in a similar direction for the scenarios 3 and 4, together with the sea state averaged wave steepness (Table 8).

The optimal slope length is related to the slope angle and the crest freeboard [Equations (33) and (34)] and consequently depends on both the sea state averaged wave height and wave steepness. The combination of both parameters results in an increase in optimal slope length from Ostend to MPN, and in a small decrease in optimal slope length from MPN to Fjaltring.

Furthermore, it appears that the optimal crest freeboard and slope angle of scenario 4 (fixed slope angle and crest freeboard) are approximately equal to the crest freeboard of scenario 2 (fixed crest freeboard) and the optimal slope angle of scenario 3 (fixed slope angle) respectively. Both similarities

are due to the limited effect of the slope angle on the average overtopping rate (and thus on the overall hydraulic efficiency and power) for $1.5 < \cot \alpha < 2.8$.

4.3. Effect of Different Geometry Control Scenarios on Overall Hydraulic Efficiency

The overall hydraulic efficiency has been calculated based on Equation (1) for each of the five scenarios at the three possible deployment sites. The resulting graph for Ostend is shown in Figure 8.

The mean overall hydraulic efficiency corresponding to the fixed geometry of scenario 4 is 15.3% for the deployment site in Ostend. Applying an adaptive slope angle (S2) increases the mean overall hydraulic efficiency up to 16.8%, while applying an adaptive crest freeboard (S3) results in a mean efficiency of 18.9%. This shows that the effect of an adaptive crest freeboard on the overall hydraulic efficiency is much larger than the effect of an adaptive slope angle. The explanation for this observation is found in the weak dependency of the average overtopping rate on the slope angle in the zone around the optimal slope angle. The fixed slope angle of the fixed geometry deviates from the optimal slope angle, but since the effect of the slope angle on the average overtopping rate is rather small, the effect of this deviation is limited compared to the effect of deviations in crest freeboard.

Figure 8. Comparison between effects of five scenarios on the overall hydraulic efficiency for test site in Ostend, Belgian Continental Shelf.
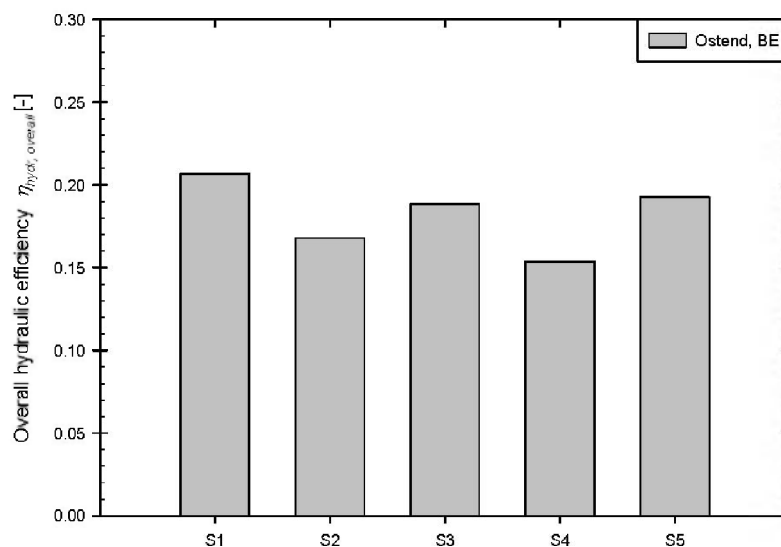
Compared to the scenario of an adaptive crest freeboard, the mean overall hydraulic efficiency can be increased by applying an adaptive crest freeboard with a hinge at the bottom of the slope (S5), up to a value of 19.3%. This value is larger than for scenario 3, due to the positive effect of the slope angle. The largest mean overall hydraulic efficiency is achieved when combining an adaptive slope angle and an adaptive crest freeboard (S1): 20.7%.

Figure 9. Comparison between mean overall hydraulic efficiency of scenario 1 for test sites in Ostend, MPN and Fjaltring.
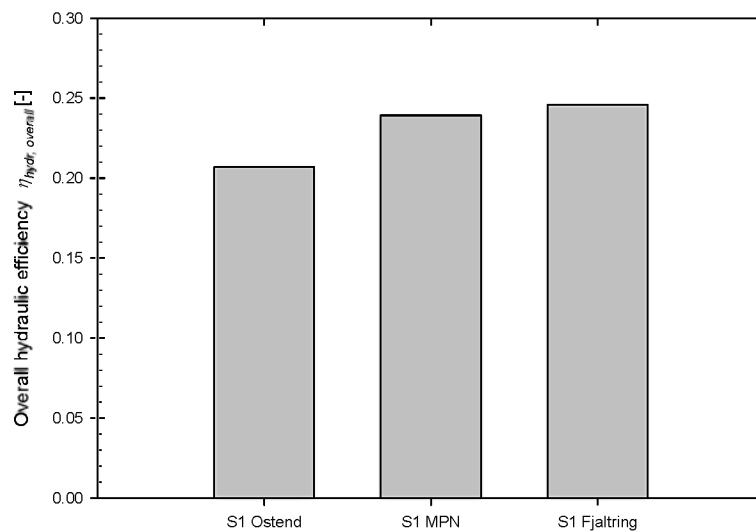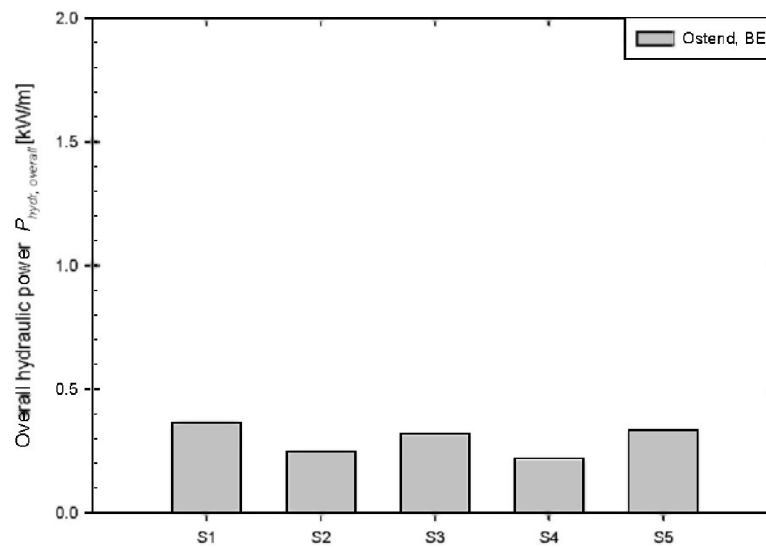

Similar graphs have been generated for the possible deployment sites at MPN, NL and Fjaltring, DK (see Appendix A). Based on these figures, the conclusions for the other two sites are similar to the conclusions for Ostend. The general conclusion thus is drawn that an adaptive crest freeboard increases the overall hydraulic efficiency considerably, while an adaptive slope angle only has a small effect. Similar conclusions are expected to be valid for the overall hydraulic power. Since power is more tangible than efficiency, the gain in overall hydraulic power by using geometry control is explicitly studied in Section 4.4.

The difference in mean overall hydraulic efficiency for scenario 1 between the different deployment sites is shown in Figure 9. It appears that the mean overall hydraulic efficiency increases when moving from Ostend to Fjalting over MPN. A relatively large difference occurs between Ostend and the other two sites. This trend is similar to the trend of the sea state averaged wave steepness given in Table 7.7. The relationship between the wave steepness and the overall hydraulic efficiency for scenario 1 is given in Equation (21c), thus explaining the differences in Figure 9.

4.4. Effect of Different Geometry Control Scenarios on Overall Hydraulic Power

The mean overall hydraulic power obtained based on Equation 5 for each of the scenarios is shown in Figure 10 for the deployment site in Ostend. The mean overall hydraulic power for scenario 4 equals 0.22 kW/m. Compared to this fixed geometry, applying an adaptive slope angle increases the mean power by 12% up to 0.25 kW/m, while applying an adaptive crest freeboard increases the mean power by 45% up to 0.32 kW/m. This confirms the larger effect of the relative crest freeboard compared to the effect of the slope angle around its optimum. The gained mean overall hydraulic power can be further increased by applying an adaptive crest freeboard with a hinge at the bottom of the slope (scenario 5) due to the positive effect of the slope angle. The increase is 52% compared to the fixed scenario, up to a value of 0.34 kW/m. The largest mean overall hydraulic power is achieved when combining an adaptive slope angle and an adaptive crest freeboard. The power is increased by 65% to 0.36 kW/m.

Figure 10. Comparison between effects of five scenarios on the overall hydraulic power for test site in Ostend, Belgian Continental Shelf.

Similar graphs have been generated for the deployment sites at MPN, NL and Fjaltring, DK (Appendix B). The conclusions are similar to the conclusions for Ostend. Scenario 5 corresponds to an increase in mean overall hydraulic power by 56% for the test location at MPN. The increase in mean overall hydraulic power when applying scenario 5 instead of scenario 4 in Fjaltring is smaller: 30%. Furthermore, the effect of an adaptive slope angle is very small and even results in a decrease in the mean overall hydraulic power. The reason for the small effect of the slope angle is the relatively small variation in wave steepness between the dominating sea states in Fjaltring. Consequently, the differences between the mean overall hydraulic power for scenarios 1, 3 and 5 are also relatively small. The differences between scenario 1, 3 and 5 on the one hand and scenario 4 on the other hand are relatively small compared to the deployment sites in Ostend and at MPN. This means that the crest freeboard in scenario 4 is closer to the values of the optimal crest freeboards of a large part of the sea states in Fjaltring. Based on Table 6, the waves at Fjaltring are dominated by three sea states with relatively small differences in wave height and in frequency of occurrence. The fixed crest freeboard for scenario 4 approximately fulfils $R_{c,j}/H_{m0,j} = 0.56$ for the sea states with the largest frequencies of occurrence. Since the site in Fjaltring is dominated by three sea states, compared to one sea state in Ostend and at MPN, the effect of geometry control is smaller in Fjaltring than at the other two sites.

In conclusion, an adaptive crest freeboard increases the overall hydraulic power for OWECs. Scenario 5, with the hinge at the bottom of the slope, is the best practically realizable scenario. In order to have an idea about the obtained hydraulic power of the single reservoir OWECs considered in this paper, the following two graphs have been generated. The increase in overall hydraulic efficiency between the traditional scenario (scenario 4) and scenario 5 is shown in Figure 11 for all three possible deployment sites.

Figure 11. Comparison between overall hydraulic power for scenario 4 and 5 at all three test sites.
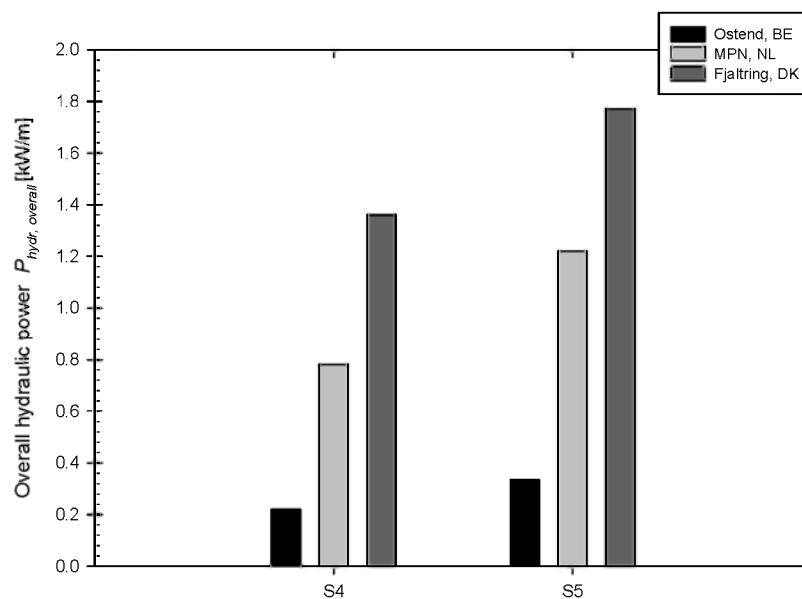
For example in Fjaltring, applying scenario 5 increases the mean overall hydraulic power from 1.4 kW/m (S4) to 1.8 kW/m. This means, for an OWEC with a length of 100 m (Figure 12) installed in Fjaltring that applying a hinge at the bottom of the slope results in an obtained power of approximately 180 kW instead of 140 kW. In Ostend, the overall hydraulic power obtained for an OWEC with a length of 100 m applying scenario 5 is approximately 35 kW.

Figure 12. Comparison between overall hydraulic power [kW] gathered over a length of 100 m for scenario 4 and 5 at all three test sites.
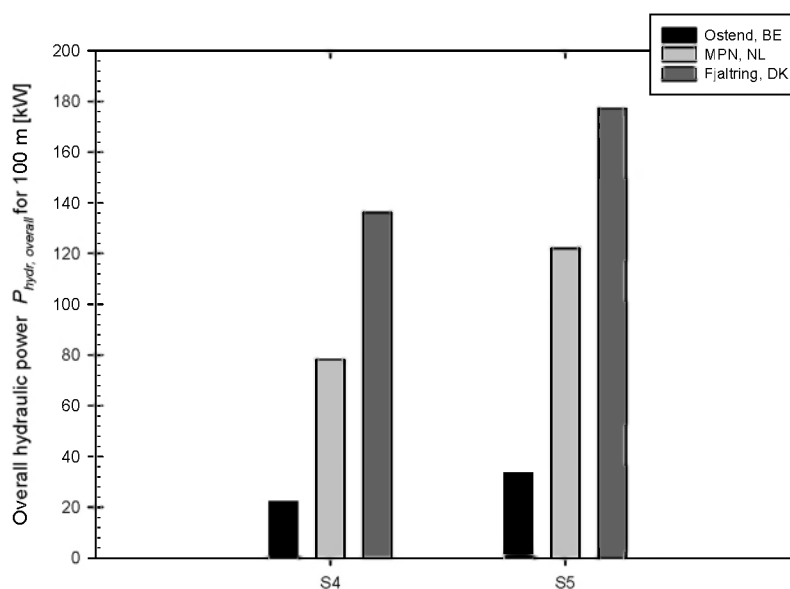
5. Conclusions

For the purpose of optimizing the performance of overtopping wave energy converters (OWECs), the effect of geometry control on the performance of OWECs deployed in wind seas (no swells) has been studied. For a particular sea state (subscript *j*), the performance of a single reservoir OWEC with a slope extending to the seabed is specified by the product of the average overtopping rate q_j and the crest freeboard $R_{c,j}$ of the OWEC. The average overtopping rate is governed by the slope angle and relative crest freeboard of the OWEC and predicted by a set of empirical formulae which have been derived based on recently achieved experimental test results (UG10 dataset). Geometry control consists of adapting the slope angle and crest freeboard of the OWEC to each sea state to obtain a maximum value of $q_j R_{c,j}$ for each sea state, resulting in a maximum hydraulic efficiency. The optimal slope angle for a sea state is determined by the condition $\tan\alpha_j = 3.0\sqrt{s_{m-1,0,j}}$, while the optimal crest freeboard should fulfil $R_{c,j}/H_{m0,j} = 0.56$. The corresponding maximum hydraulic efficiency is only dependent on the wave steepness.

However, since applying such optimal geometry is not straightforward, four additional scenarios have been studied, which correspond to a more simplified control of the geometry. These scenarios include the traditional fixed scenario without geometry control, *i.e.*, with a fixed slope angle and a fixed crest freeboard.

The overall hydraulic efficiency and overall hydraulic power have been calculated based on the empirical formulae of the UG10 dataset for each of the five scenarios for OWECs at three possible deployment sites: Ostend (Belgian Continental Shelf), MPN (Dutch Continental Shelf) and Fjaltring (Danish Continental Shelf). The sites have been chosen based on their water depth and their variety in characteristic sea states.

These simulations allow one to verify whether increases in overall hydraulic efficiency and overall hydraulic power can be achieved when controlling the geometry compared to a fixed geometry. It appears that applying an adaptive crest freeboard considerably increases the obtained overall hydraulic efficiency and power. The best practically realizable scenario corresponds to the installation of a hinge at the bottom of the slope and to apply an adaptive crest freeboard control strategy. Based on the simulations, the gain in overall hydraulic power for that scenario compared to a fixed geometry is at least 30%. This shows that applying geometry control should be considered in the design and feasibility of overtopping wave energy converters.

Acknowledgments

Appendix A: Effect of Geometry Control on Overall Hydraulic Efficiency—MPN and Fjaltring

Figure A1. Comparison between effects of five scenarios on the overall hydraulic efficiency for test site at MPN, Dutch Continental Shelf.
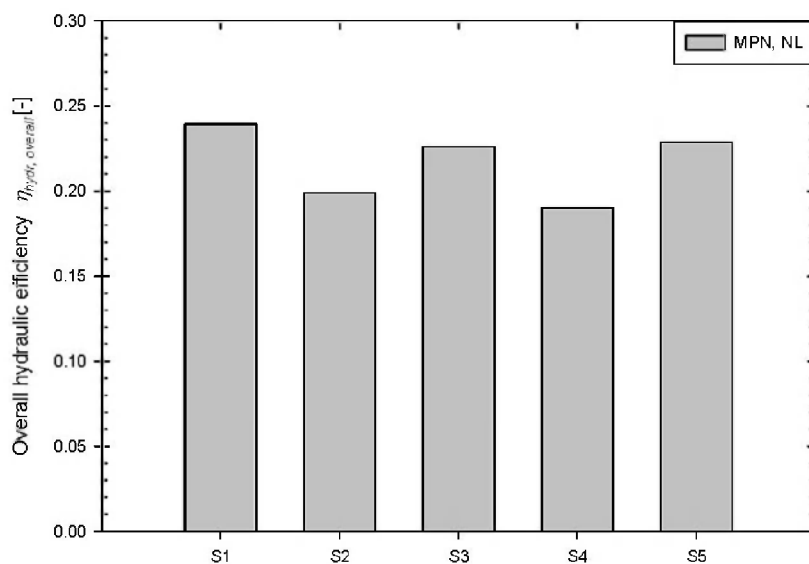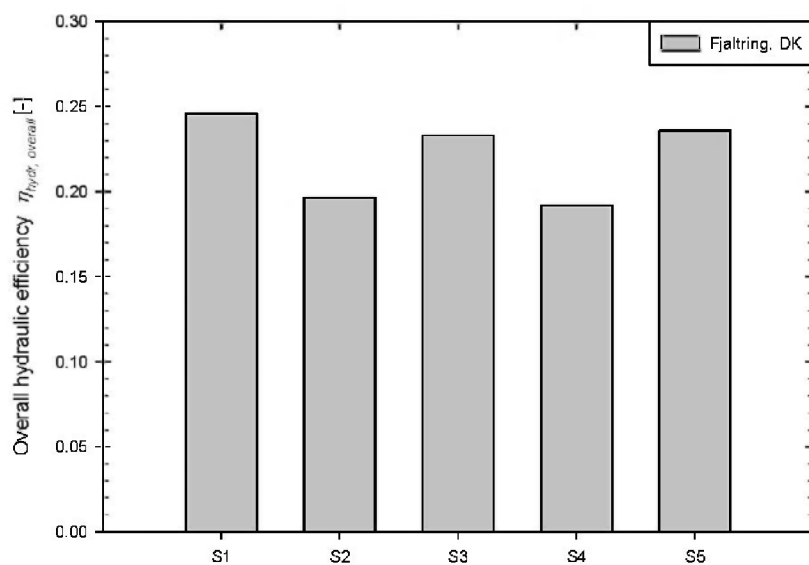

Figure A2. Comparison between effects of five scenarios on the overall hydraulic power for test site in Fjaltring, Danish Continental Shelf.

Appendix B: Effect of Geometry Control on Overall Hydraulic Power—MPN and Fjaltring

Figure B1. Comparison between effects of five scenarios on the overall hydraulic power for test site at MPN, Dutch Continental Shelf.
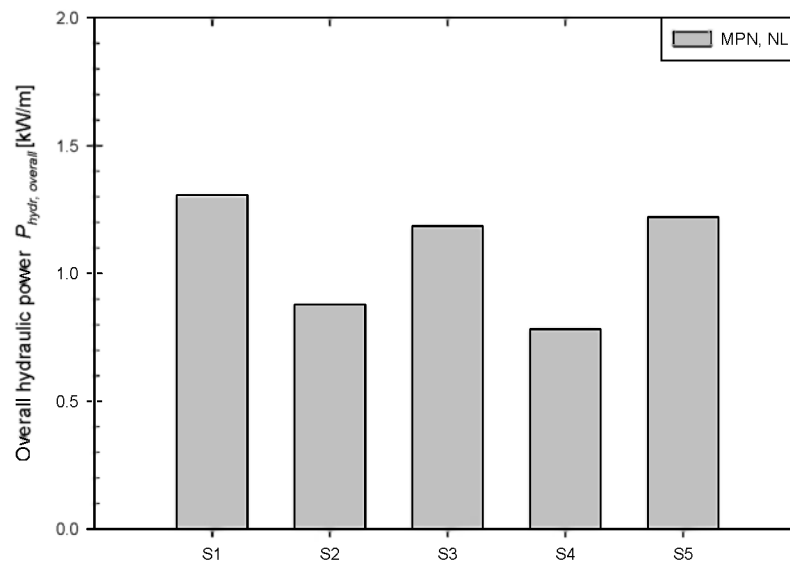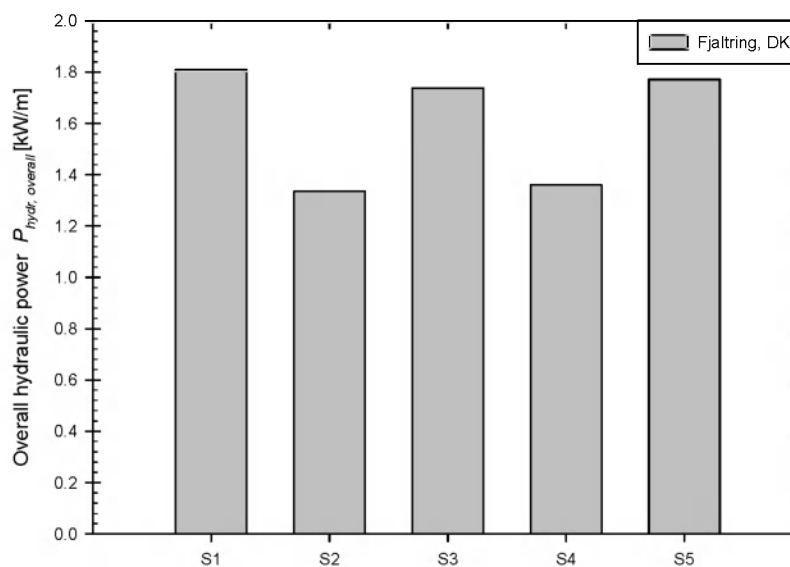

Figure B2. Comparison between effects of five scenarios on the overall hydraulic power for test site in Fjaltring, Danish Continental Shelf.

References

1. Kofoed, J.P. Wave Overtopping of Marine Structures—Utilization of Wave Energy. Ph.D. Dissertation, Aalborg University, Aalborg, Denmark, 2002.
2. Margheritini, L.; Victor, L.; Kofoed, J.P.; Troch, P. Geometrical Optimization for Improved Power Capture of Multi-Level Overtopping based Wave Energy Converters. In *Proceedings of the Nineteenth (2009) International Offshore and Polar Engineering Conference (ISOPE)*, Osaka, Japan, 21–26 June 2009; International Society of Offshore & Polar Engineers: Osaka, Japan, 2009; pp. 339–344.
3. van der Meer, J.W.; Janssen, J.P.F.M. *Wave Run-up and Wave Overtopping at Dikes and Revetments*; Delft Hydraulics: Delft, The Netherlands, 1994.
4. Pullen, T.; Allsop, N.W.H.; Bruce, T.; Kortenhaus, A.; Schüttrumpf, H.; van der Meer, J. *EurOtop—Wave Overtopping of Sea Defences and Related Structures: Assessment Manual (2007)*. Available online: http://www.overtopping-manual.com (accessed on 18 October 2011).
5. Schüttrumpf, H. Wellenüberlaufströmung bei Seedeichen—Experimentelle und Theoretische Untersuchungen. Ph.D. Dissertation, Technischen Universität Carolo-Wilhelmina, Braunschweig, Germany, 2001.
6. Victor, L.; Troch, P. Wave overtopping at smooth impermeable steep slopes with low crest freeboards. *J. Waterw. Port Coast. Ocean Eng.* **2011**, submitted.
7. Victor, L.; Troch, P. Development of a Test Set-up to Measure Large Wave-by-Wave Overtopping Masses. In *Proceedings of the Third International Conference on the Application of Physical Modelling to Port and Coastal Protection (Coastlab 10)*, Barcelona, Spain, 28 September–1 October 2010.
8. Franco, L.; de Gerloni, M.; van der Meer, J. Wave Overtopping on Vertical and Composite Breakwaters. In *Proceedings of the 24th International Conference on Coastal Engineering*, Kobe, Japan, 23–28 October 1994; ASCE: New York, NY, USA, 1994; pp. 1030–1044.
9. Rijkswaterstaat Golfklimaat. National Institute for Coastal and Marine Management (rijkswaterstaat), The Netherlands. Available online: http://www.golfklimaat.nl (accessed on 20 July 2010).
10. Rambøll; Dansk Hydraulisk Institut; Danmarks Meteorologiske Institut. *Kortlaegning af Bolgeenergiforhold i den Danske del af Nordsoen*; Energistyrelsen: Copenhagen, Denmark, 1999.